A STUDY OF A TINY TWO-RIBBON FLARE DRIVEN BY EMERGING FLUX

Takuma Sakajiri,[1,2] David H. Brooks,[1] Tetsuya Yamamoto,[1,2] Daikou Shiota,[1,2] Hiroaki Isobe,[1]
Sachiko Akiyama,[1,3] Satoru Ueno,[1] Reizaburo Kitai,[1] and Kazunari Shibata[1]

ABSTRACT

We present observations of the eruption of a miniature filament that occurred near NOAA Active Region 9537 on 2001 July 14. The eruption was observed by the Hida Observatory Domeless Solar Telescope, in the Hα line center and ±0.4 Å wings, the *Solar and Heliospheric Observatory* EUV Imaging Telescope (EIT) and Michelson Doppler Imager, and the *Yohkoh* Soft X-Ray Telescope (SXT). The miniature filament began to form and was clearly visible in Hα images by around 06:50 UT. It erupted about 25 minutes later, accompanied by a small two-ribbon subflare (with an area of 61 arcsec^2). The two ribbons were also found to approach each other at a speed of 3.33 km s^{-1}. We found that this event was caused by the emergence of new magnetic flux in a quiet region. The emerging flux appeared as a bright region in the EIT and SXT images taken on the previous day. It moved southward into an area of preexisting opposite-polarity flux, where a cancelling magnetic flux region was formed. The miniature filament then appeared, and we suggest that it played some role in inhibiting the release of energy by delaying reconnection between the emerging and preexisting flux, as evidenced by the disappearance of the bright region between opposite polarities in the EUV and soft X-ray images. Consequently, magnetic energy was stored as a result of the slow converging motion of the two opposite-polarity flux regions (0.17 km s^{-1}). Reconnection below the filament provoked the filament eruption, and the two-ribbon flare occurred. Miniature filaments are thought to be small-scale analogs of large-scale filaments. Our observations also suggest some common properties between small-scale and large-scale flares. These results support the view that a unified magnetic reconnection model may be able to explain all scales of flares.

Subject headings: Sun: filaments — Sun: flares — Sun: magnetic fields

Online material: color figures

1. INTRODUCTION

Miniature filament eruptions have been studied for many years. Moore et al. (1977) and Labonte (1979) were the first authors to describe limb and disk events, respectively. However, Hermans & Martin (1986) made the first comprehensive study of these events as a separate class using Hα observations from the Big Bear Solar Observatory (BBSO). They concluded that eruptive miniature filaments are the small-scale analogs of large-scale eruptive filaments. More recently, Wang et al. (2000) studied BBSO Hα filtergrams and clarified some basic characteristics of miniature filament eruptions. For example, (1) the eruptive miniature filaments lie above the magnetic polarity reversal boundaries between adjacent opposite-polarity fields, (2) they are spatially correlated with cancelling magnetic features at these boundaries, (3) their morphological evolution implies that they are most likely magnetic loops, (4) they appear much less stable (in form and brightness) than their large-scale analogs, (5) almost all miniature filament eruptions are associated with tiny flares that are brightest during the activation phase, and (6) the brightenings during the small flares appear very similar to the two-ribbon/multiribbon flares associated with large-scale eruptive filaments.

Many aspects of Hα two-ribbon flares can be explained by the standard (CSHKP) magnetic reconnection model

(Carmichael 1964; Sturrock 1966; Hirayama 1974; Kopp & Pneuman 1976) and its modern extension (Forbes & Priest 1982; Cargill & Priest 1983; Cliver 1983; Martens & Kuin 1989; Moore & Roumeliotis 1992; Svestka & Cliver 1992). In addition, considering the observational evidence for magnetic reconnection provided by the *Yohkoh* satellite, Shibata (1996, 1998, 1999) presented a unified model of flares: the plasmoid-induced reconnection model. This model attempts to draw together a variety of solar activities and explain them within the same unified framework. Shibata (1999) showed that such a model could be applied to a wide range of solar active phenomena of different timescales and sizes, e.g., transient brightenings associated with Hα surges, impulsive compact loop flares, long-duration event flares, and giant arcade formation associated with coronal mass ejections. A similar idea has also been proposed by Moore et al. (1999) and Falconer et al. (2003). Therefore, a further question arises with regard to the miniature filament eruptions and the similarity between their associated tiny flares and the two-ribbon flares of larger scale eruptive filaments, i.e., can this unified view of solar flares also be applied to such small-scale activity? This is the subject of the present paper. We examine in detail the spatial and temporal development of the miniature filament eruption and associated two-ribbon flare that occurred on 2001 July 14, using Hα, EUV, and soft X-ray images. Our objective is to study the morphology and dynamics of such small-scale solar phenomena and determine whether the unified magnetic reconnection model can explain the findings. Strictly speaking, since the area of the Hα flare is about 61 arcsec^2, this tiny event should be classified as a subflare on the solar flare optical classification scheme. It is also found to be below *GOES*

[1] Kwasan and Hida Observatories, Kyoto University, Yamashina-ku, Kyoto 607-8471, Japan; shibata@kwasan.kyoto-u.ac.jp.
[2] Department of Astronomy, Kyoto University, Sakyo-ku, Kyoto 606-8502, Japan.
[3] Institute for Computational Sciences and Informatics, George Mason University, Fairfax, VA 22030.
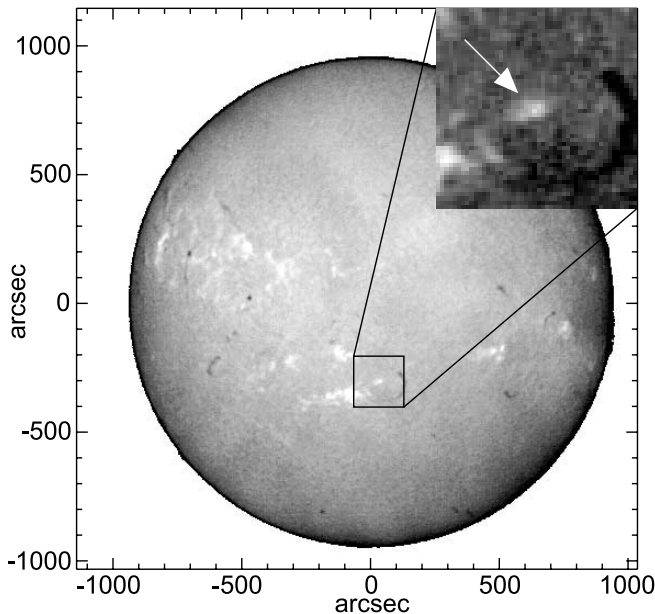
FIG. 1.—Hα full-Sun image with the Hida Observatory FMT at 07:15:00 UT on 2001 July 14. A small flare occurred just below disk center, and a close-up image of the flaring region is shown in the top right corner of the figure. An arrow indicates the location of the flare.
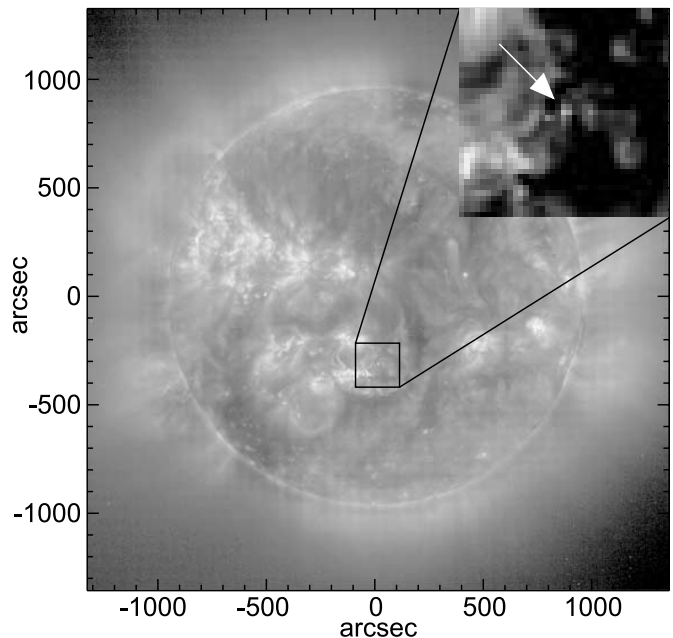

FIG. 2.—EIT Fe XII λ195 full-Sun image of the same flare. An arrow again indicates the location of the flare in a close-up image.

class C1. However, in subsequent sections we refer to it simply as a flare, since the paper is primarily concerned with the possibility of the unification of all scales of flares.

In § 2 we briefly describe the details of the observations we analyzed. In § 3 we present the results of our analysis. Finally, in § 4 we summarize and discuss the findings.

2. OBSERVATIONS

The small-scale two-ribbon flare associated with the miniature filament eruption occurred near NOAA Active Region 9537 on 2001 July 14 at around 07:13 UT. The development of the event was recorded by the 60 cm Domeless Solar Telescope (DST) at Kyoto University's Hida Observatory, which observed between 06:00 and 07:27 UT. Hα monochromatic images were obtained with the Zeiss Lyot filter (with a passband of 0.25 Å) and the Nikon motor-drive film camera installed on the DST. Images in eight wavelengths around Hα line center were obtained. However, in this study we only used the observations at line center and ±0.4 Å. The two-ribbon flare and miniature filament eruption were clearly visible in the images at these wavelengths, so we judged that they were sufficient for analyzing the event. In this paper, as a context image for displaying the location of the event, we also used one full-Sun Hα line center image taken by the Flare Monitoring Telescope (FMT) at Hida Observatory (Kurokawa et al. 1995).

To study the multiwavelength spatial and temporal development and magnetic field evolution of this event, we also analyzed EUV and soft X-ray images obtained by the *Solar and Heliospheric Observatory* (*SOHO*) EIT (Delaboudiniére et al. 1995) and *Yohkoh* SXT (Tsuneta et al. 1991), together with photospheric magnetograms obtained by the *SOHO* MDI (Scherrer et al. 1995). SXT and EIT Fe XII λ195 images of the region were available in their respective archives for the period from 01:40 UT on July 13 to 07:30 UT on July 14. The SXT images were obtained with the thin aluminium filter (Al.1). However,

unfortunately, no SXT images were recorded at the time of the small two-ribbon flare.

3. RESULTS

3.1. Hα Observations

Figures 1 and 2 show the location of the flare on full-disk images in the Hα line center taken with the FMT and an Fe XII λ195 image taken with EIT, respectively. The Hα image was taken at 07:15 UT, and the EIT image was taken at 07:24:18 UT. The flare occurred near NOAA AR 9537, which was positioned a little to the south of the disk center. A $200'' \times 200''$ cutout region surrounding the flare is also shown in close-up in the top right corner of each figure, and the area is outlined by a box on the full-disk image. White arrows in the zoomed images indicate the flare we studied.

Figure 3 shows the temporal evolution of the miniature filament eruption and two-ribbon flare at high spatial resolution in the Hα line center and ±0.4 Å red and blue wings observed by the DST during the period from ∼06:57 to ∼07:25 UT. The area is the $56''$ square cutout of the zoomed images of Figure 1. The Hα line center and red/blue-wing images are all obtained through the same filter, so the co-alignment accuracy is expected to be at the $1''-2''$ level (depending on seeing conditions).

Note the presence of the small-scale filament in the Hα line center image at 07:13:58 UT. It began to form before or around 6:30 UT, but the seeing conditions at that time (and also because the filament was so small) made it difficult to accurately determine the start time. However, by around 6:50 UT it is clearly visible. At the time of the 7:13:58 UT image, the filament has also begun to rise, and it is visible in the −0.4 Å blue-wing image at 07:13:55 UT. Around the same time, the two ribbons of the small-scale flare began to brighten in all three wavelengths. Note the two bright ribbons below the west (right) end of the filament that appear very faintly in the images around 07:14 UT and are clearly visible in the images around 07:14:30 UT. Around 07:16 UT the flare ribbons reach their
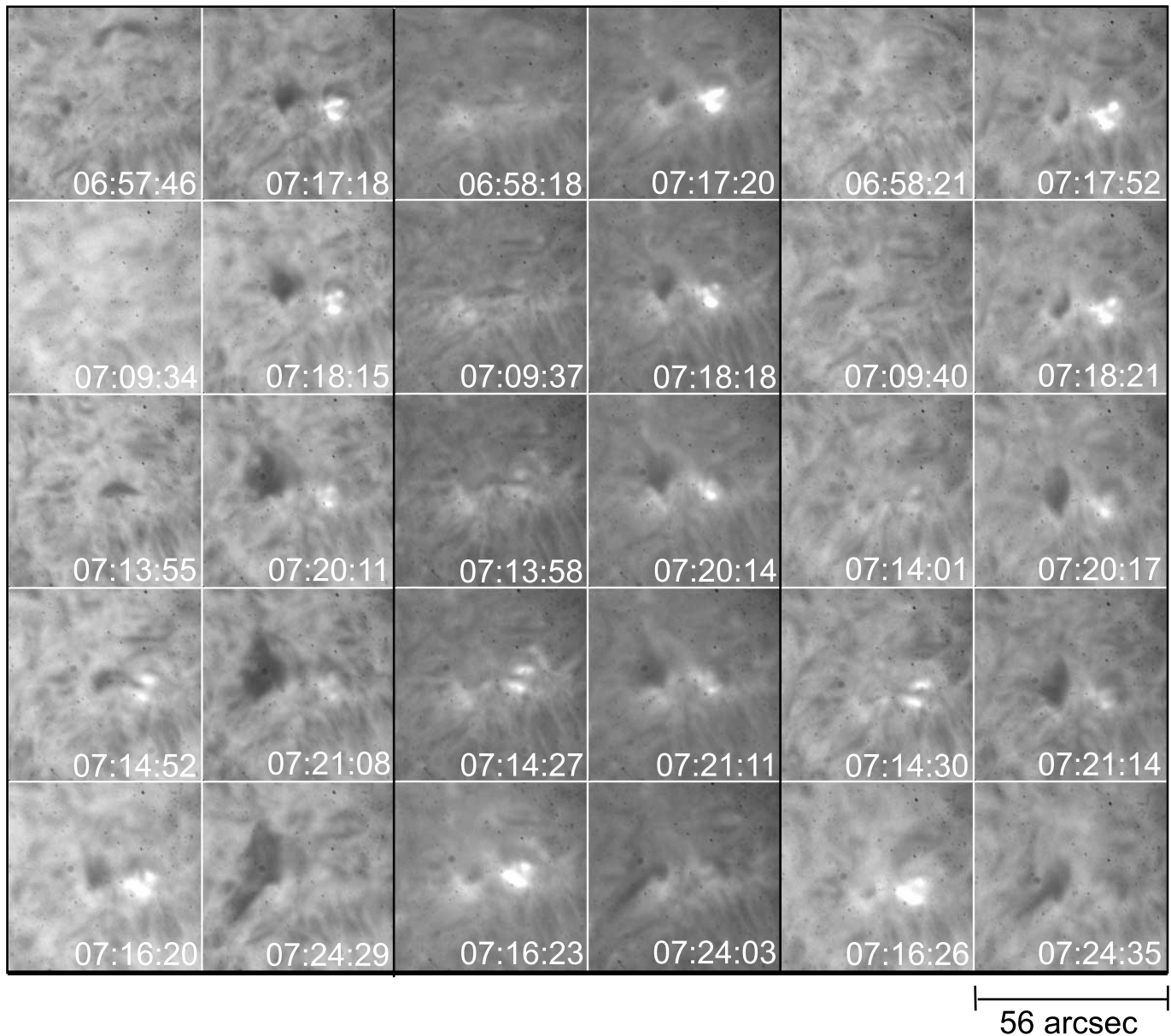
FIG. 3.—Temporal development of the miniature filament and two-ribbon flare between 06:57:46 and 07:24:35 UT in Hα − 0.4 Å (*left two columns*), line center (*middle two columns*), and +0.4 Å (*right two columns*) images. The area is 56″×56″.

maximum brightness during the event. Note also that the ribbons appear to show more detailed structure at this time, i.e., a third ribbon appears to separate out from the lower one. The rising filament also separates into two distinct regions (east and west). See, for example, the −0.4 Å blue-wing image taken at 07:17:18 UT. In addition, note that the westerly component of the separated filament moves to cover and obscure the flare ribbons (see, e.g., the 07:20:14 UT line center image). In contrast, the easterly component continues in that direction and appears to fragment and scatter. Subsequently, a great deal of "scattered" plasma is visible in all wavelengths (see the final images of Fig. 3).

Figure 4 shows the spatial relationship between the dark features observed in the Hα line center and blue and red wings. The left panel shows the line center image and was taken at 07:18:18 UT, just after the peak brightness of the flare ribbons. The dark features in nearly simultaneous Hα −0.4 and +0.4 Å images are overlaid as dark and light contours, respectively.

The blue-wing image was taken at 07:18:15 UT, and the red-wing image was taken at 07:18:21 UT. The area in both panels of the images is approximately 65″×65″. The right panel shows the same layout but with the line center image taken at 07:24:03 UT, the blue wing at 07:24:29 UT, and the red wing at 07:24:35 UT.

Note how the rising and falling material is spatially coincident with opposite edges of the easterly part of the separated filament in the image at 07:18 UT. This dark structure has elongated and spread by 07:24 UT, and the Doppler shift contours for both line-of-sight motions have also stretched but continue to appear to be positioned at opposite edges. This spatial pattern of upflowing and downflowing material may be an indication that the ejected material is rotating, which has previously been observed in larger erupting filaments by Kurokawa et al. (1987). The westerly part of the separated filament does not coincide with any contours at 07:18 UT, but by 07:24 UT a light contour appears to surround part of this
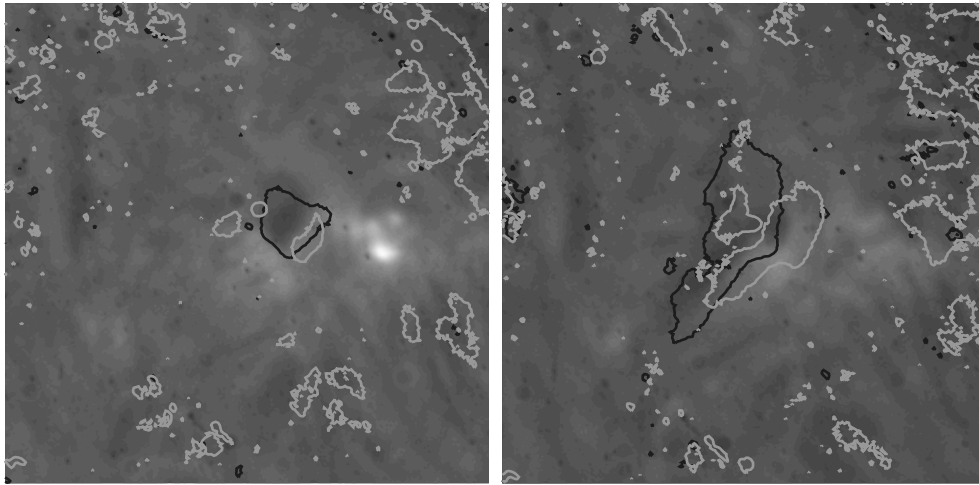
FIG. 4.—Hα line center images of the miniature filament eruption with intensity contours (*dark and light, respectively*) of the dark features in nearly simultaneous blue- and red-wing images overlaid. *Left*: Hα line center image at 07:18:18 UT, with overlaid contours of the dark features in the blue- and red-wing images taken at 07:18:15 and 07:18:21 UT, respectively. *Right*: Hα line center image at 07:24:03 UT, with overlaid contours of the dark features in the blue- and red-wing images taken at 07:24:29 and 07:24:35 UT, respectively. [*See the electronic edition of the Journal for a color version of this figure.*]

structure. This is consistent with this part of the filament having been ejected horizontally to the west (so that it has mainly a horizontal component of velocity at 07:18 UT) and later falling back to the solar surface (07:24 UT). However, there are other possible scenarios that would explain the observational data. For example, another possibility is that the blueshifted component is accompanied by downflowing redshifted components both below the erupting filament and also farther to the west.

Using the Hα line center images, we determined the size of the flare by defining it as the area where the intensity was greater than 60% of the maximum intensity. Thus, we found a value of about $7\farcs8 \times 7\farcs8$ (i.e., $\sim$61 arcsec^2). We also determined the distance between the two flare ribbons and the variation of this value between 07:14 and 07:21 UT. The result is displayed
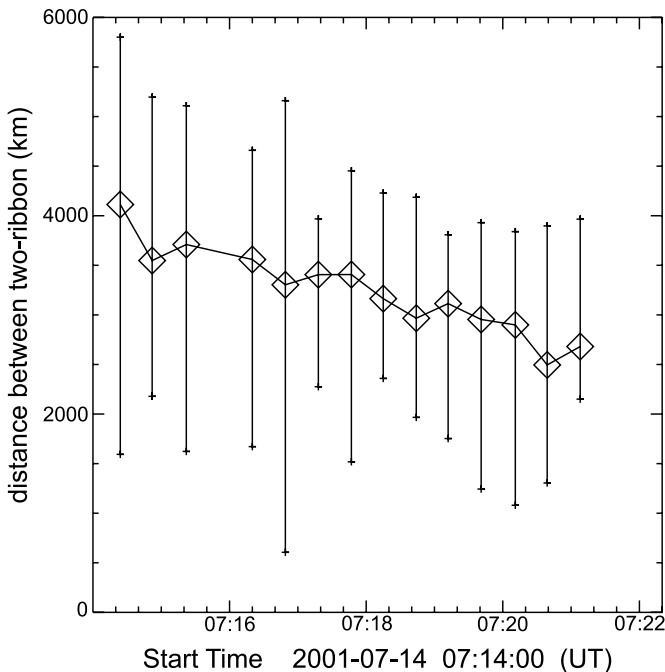

FIG. 5.—Temporal variation of the distance between the two ribbons. The convergence speed is approximately 3.33 km s^{-1}.

in Figure 5. The abscissa of the coordinate frame shows the time, and the ordinate shows the distance between the ribbons (*diamonds*) as measured from the Hα images. The error bars provide an estimate of the upper and lower limits to the derived values by estimating the distances between the outer and inner edges of the two ribbons. It can be seen that the two ribbons converged during this 7 minute period, and the closing speed is approximately 3.33 km s^{-1}.

3.2. *MDI, EIT, and SXT Observations*

First, we examined the development of the photospheric magnetic field in the flaring region from about 33 hr prior to the flare until about 5 hr after. Figure 6 shows MDI magnetograms taken at 22:23 UT on July 12, 01:35, 09:35, and 19:11 UT on July 13, and 06:27 and 12:47 UT on July 14. A horizontal scale bar showing a length of 60″ is displayed in the bottom right of the figure. The red contours show positive magnetic flux, and the blue contours show negative values. The contours are for -150, -100, -50, 30, 50, and 100 G. The emerging flux region begins to appear around 22:23 UT on July 12 (note the small positive-polarity contours in the east side of the image just above the center) and is clearly visible in the 01:35 UT magnetogram. It is difficult to distinguish the emerging negative-polarity companion flux in the magnetograms. This may suggest that it is located in the preexisting negative field. The positive flux region begins to cancel the preexisting negative magnetic field (to the west side) and approach this region at a speed of 0.17 km s^{-1}. This is much slower than the converging speed estimated for the two ribbons (3.33 km s^{-1}), implying that the motion of the two ribbons is not associated with the observable motion of the photospheric magnetic field. In addition, the total unsigned magnetic flux within the region of the images, including the emerging flux region, does not change. This is further observational support for the identification of the bipolar emerging flux region. That is, since the positive-polarity region is seen to grow and its strength to increase, we can infer the presence of an emerging companion negative-polarity region so that the total unsigned magnetic flux is conserved.

Converging motion of flare ribbons has previously been reported by Canfield et al. (1996), who suggested that the
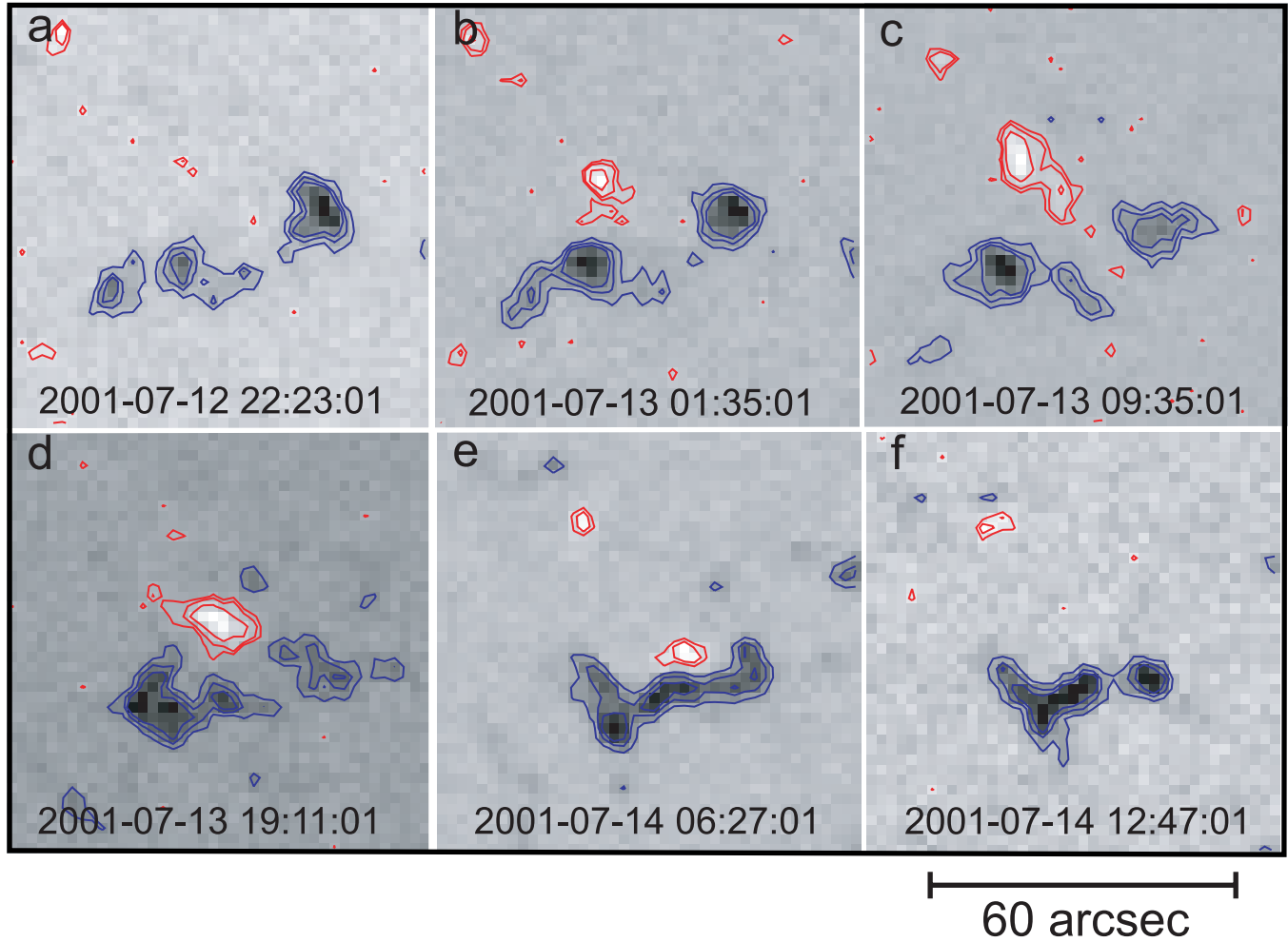
Fig. 6.—Evolution of the photospheric magnetic field in the emerging flux region observed with MDI. Red contours denote positive magnetic flux, and blue contours denote negative magnetic flux. The contour levels are -150, -100, -50, $+30$, $+50$, and $+100$ G. The positive and negative magnetic field regions were found to converge at a speed of approximately 0.17 km s^{-1}. A $60''$ horizontal bar is shown to give an indication of the size of the region.

phenomenon was associated either with emerging flux or with moving magnetic bipoles. However, they concluded that the convergence was due to brightening of the footpoints of reconnected loops formed at successive levels in the solar atmosphere, as the reconnection process between the emerging bipolar flux and preexisting field continued. The small two-ribbon flare studied in the present paper is also associated with emerging flux, which suggests a similar scenario. However, in this case we also observed a slow approach of monopolar positive-polarity flux to the preexisting region of opposite-polarity flux.

Next we examined the spatial relationship between the features observed in Hα and the magnetic field distribution. Figure 7 shows an Hα line center image taken at 07:14:55 UT on July 14 around the time when the two ribbons began to emit. The area is $50'' \times 50''$. Contours from a nearly simultaneous MDI magnetogram are overlaid (again, red is positive, and blue is negative). Contour levels of -150, -100, -50, 40, 50, and 60 G are shown. The northern and southern ribbons are clearly spatially coincident with positive and negative magnetic field contours, respectively. Furthermore, the miniature filament is clearly situated on the neutral line between opposite polarities around $X = 30$, $Y = -308$ (cf. also with, e.g., the 07:13:58 UT image in Fig. 3).

Figures 8 and 9 show EIT Fe XII λ195 images and SXT images with cotemporal photospheric magnetic field contour overlays from MDI, respectively. EIT images are shown at 01:47:59, 14:59:27, and 21:23:05 UT on July 13 and 03:46:23, 06:34:15, and 07:24:18 UT on July 14. SXT images are shown for 01:40:40, 14:31:23, and 23:12:13 UT on July 13 and 04:01:25, 06:32:29, and 07:29:49 UT on July 14. The areas are approximately $50'' \times 50''$. The 14:59:27 UT EIT image and the 14:31:23 UT SXT image, taken on the day before the flare, show the appearance of a bright region between opposite polarities during the evolution of the new magnetic flux and well before the formation of the filament. This bright region existed for several hours and is still clearly visible in the 03:46:23 UT EIT image and the 04:01:25 UT SXT image. Sometime after this, the miniature filament began to form so that the emerging flux region appeared dark in both the EUV and soft X-ray images taken around 06:30 UT. Unfortunately, *Yohkoh* did not observe the flare, but EIT obtained one image at 07:24 UT. The flare bright point can be seen between the opposite polarities.

Figure 10 shows the light curves for Fe XII λ195 and the Hα line center. The abscissa shows the time, and the ordinate shows the intensity. The Fe XII λ195 light curve was obtained using the intensity of the brightest pixel in the flare image at 7:24:18 UT. The Hα light curve was obtained using the
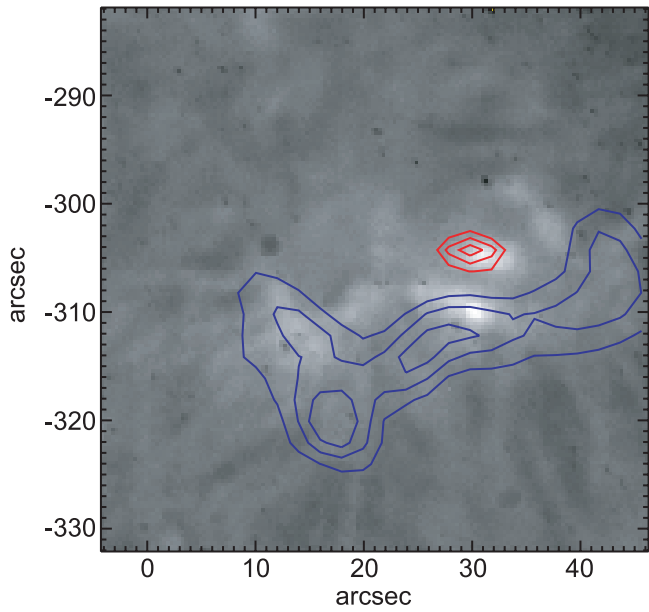
Fig. 7.—DST Hα line center image taken at 07:14:55 UT with MDI magnetogram contours overlaid. Red contours denote positive magnetic flux, and blue contours denote negative magnetic flux. The contour levels are −150, −100, −50, +40, +50, and +60 G. The area is 50″×50″.

intensity of the brightest pixel in the flare image at 7:18:46 UT. The Hα data were calibrated to the mean intensity of the images to account for changes in seeing conditions. Both intensities were then normalized to the range 0–1. The Hα curve shows a typical impulsive peak lasting around 10 minutes, and the emerging flux region (which had been dark in the EUV images) clearly brightens when the flare occurs. Although the temporal resolution of the EIT data is low, the Fe XII λ195 light curve is consistent with that of Hα.

4. SUMMARY AND DISCUSSION

We have studied in detail the spatial and temporal development of a miniature filament eruption and the associated small-scale two-ribbon flare that occurred on 2001 July 14, using observations from the DST, EIT, MDI, and SXT. Our observations clearly show that the small two-ribbon flare was associated with the cancellation of magnetic flux provoked by the emergence of new magnetic flux into a preexisting opposite-polarity field region. The main findings of our study and our interpretations can be summarized as follows (in the order in which they occurred):

1. New magnetic flux emerges, but the negative-polarity field is not seen clearly because it is located in the negative-polarity preexisting field.
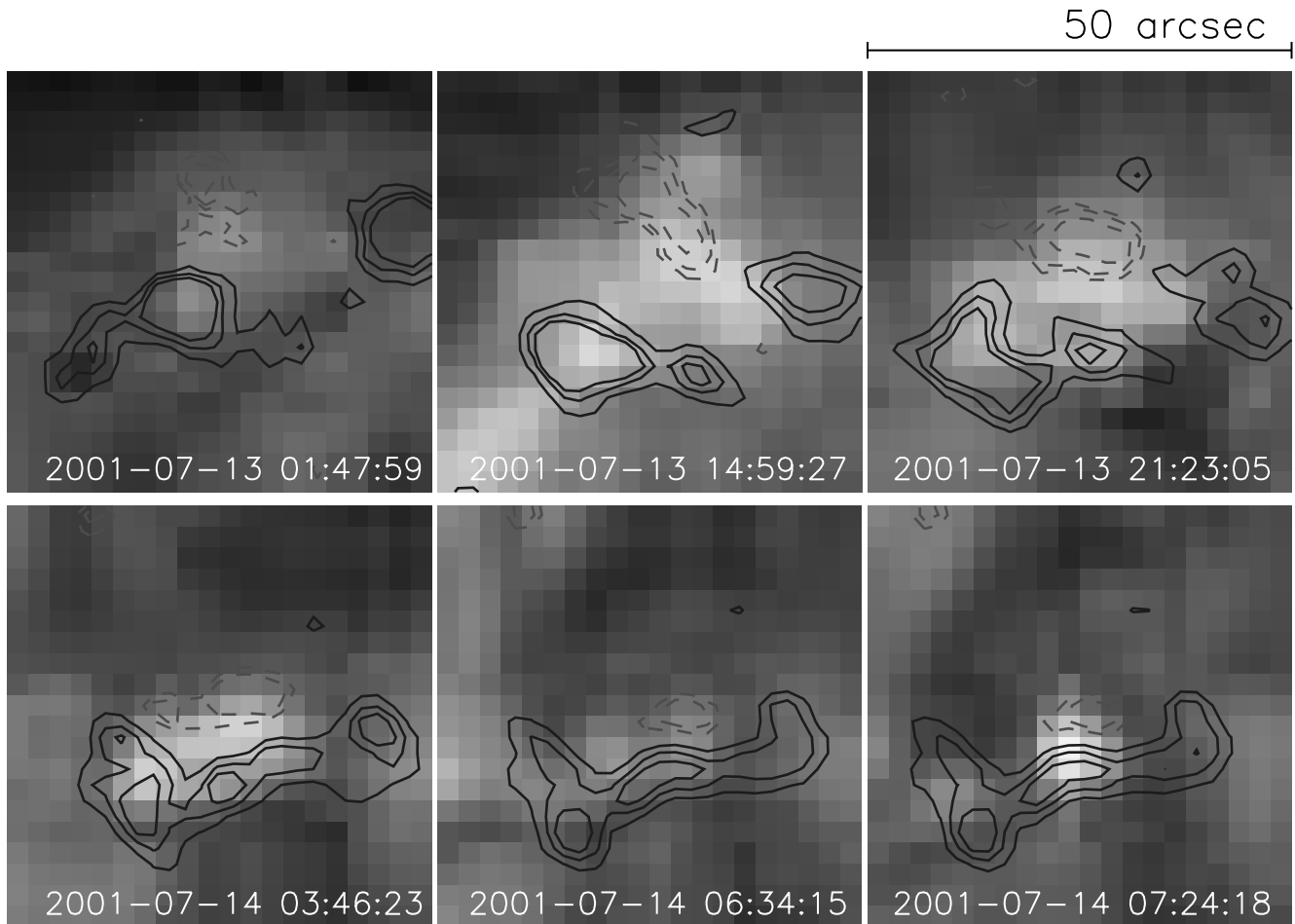

Fig. 8.—Temporal development of the region observed in Fe XII λ195 by EIT with MDI magnetogram contours overlaid. Light dotted contours denote positive magnetic flux, and dark solid contours denote negative magnetic flux. The contour levels are −150, −100, −50, +30, +50, and +100 G. The area is 50″×50″. [*See the electronic edition of the Journal for a color version of this figure.*]
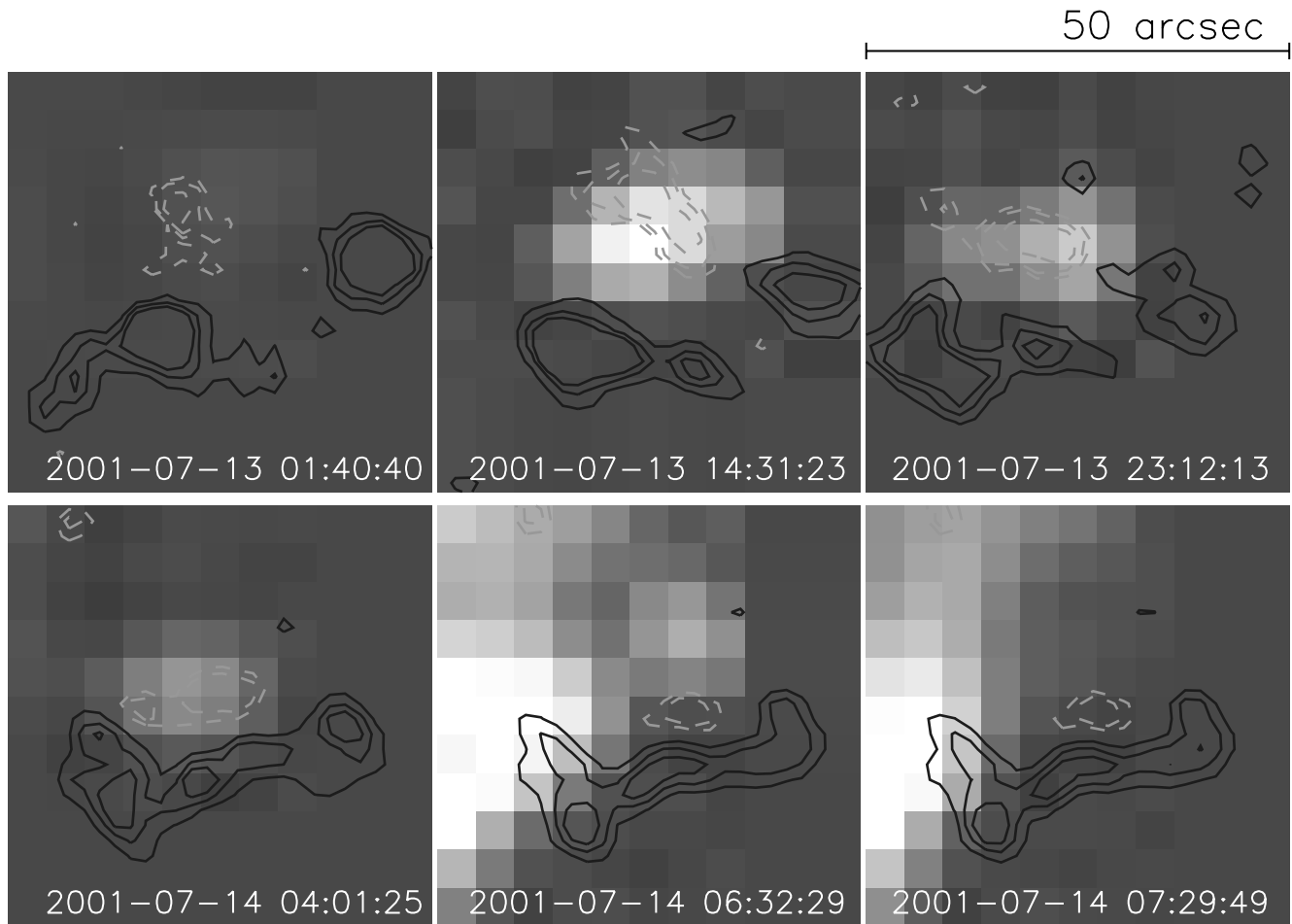
Fig. 9.—Temporal development of the region observed by the *Yohkoh* SXT with MDI magnetogram contours overlaid. Light dotted contours denote positive magnetic flux, and dark solid contours denote negative magnetic flux. The contour levels are −150, −100, −50, +30, +50 and +100 G. The size is 50″×50″. [*See the electronic edition of the Journal for a color version of this figure.*]
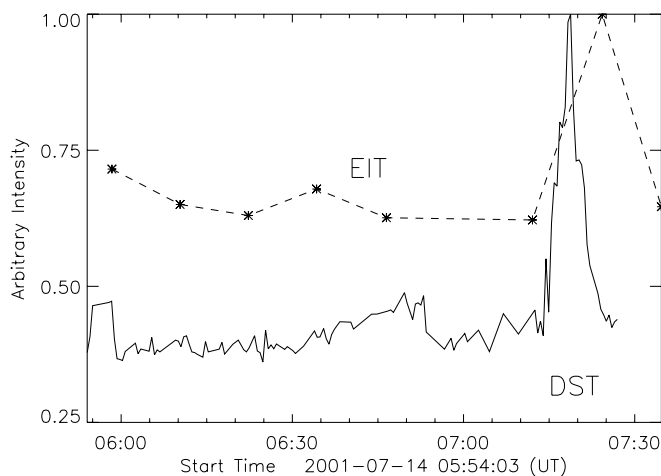

Fig. 10.—Hα and Fe xii λ195 light curves between 5:55 and 7:35 UT on 2001 July 14. The Fe xii λ195 light curve was obtained using the intensity of the brightest pixel in the flare image at 7:24:18 UT. The Hα light curve was obtained using the intensity of the brightest pixel in the flare image at 7:18:46 UT. The Hα data were calibrated to the mean intensity of the images to account for changes in seeing conditions. Both intensities were then normalized to the range 0–1.

2. The emerging flux region begins to cancel with the preexisting opposite-polarity magnetic flux region, forming a bright region between polarities in the EUV and soft X-ray images.

3. The footpoints of the two regions converge at a speed of 0.17 km s^{-1}.

4. A miniature filament forms above the neutral line between opposite polarities.

5. The formation of the miniature filament inhibits the release of magnetic energy because its formation acts to prevent continuing reconnection between the emerging flux region and the preexisting flux. This is inferred from the disappearance of the bright point between opposite polarities, in the EUV and soft X-ray images, even before the filament is clearly visible. Energy is thus stored because of the continuing convergence of the opposite-polarity regions.

6. The miniature filament erupts, showing possible rotational motion, and the energy that was stored during the miniature filament formation process is released rapidly when the small two-ribbon flare occurs.

7. The two ribbons approach each other at a speed of 3.33 km s^{-1} and subsequently show a more detailed structure, perhaps with a third ribbon separating out from the lower one.

The morphological reconnection model, shown in Figure 11, depicts one interpretation of the observational features of the data analyzed in this study. In stage 1 new magnetic flux emerges, with the negative-polarity flux located within the
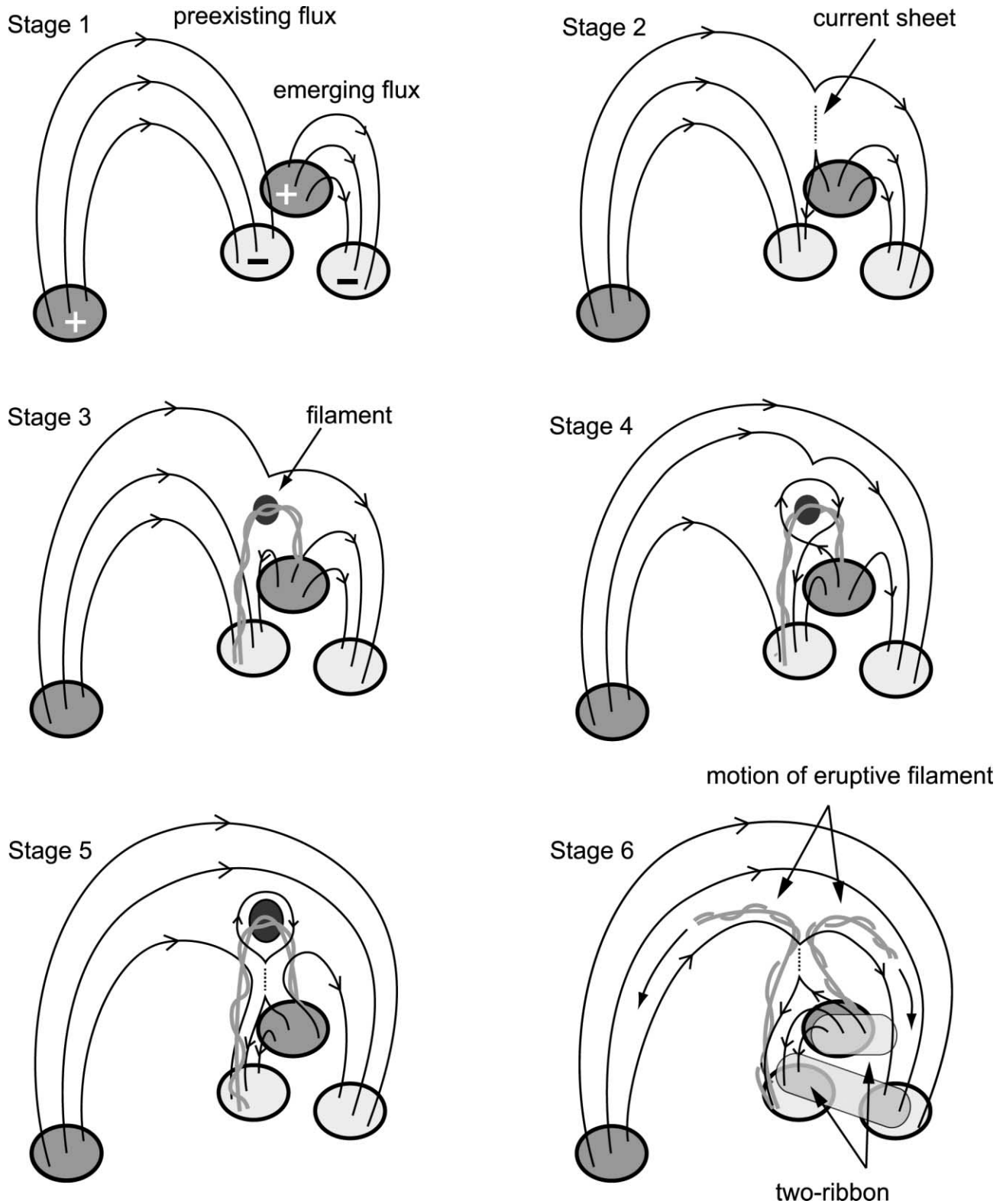
Fig. 11.—Morphological reconnection model for the event. The dark and light regions denote positive and negative magnetic flux regions, respectively. [*See the electronic edition of the Journal for a color version of this figure.*]

preexisting negative-polarity region. The positive-polarity flux of the emerging flux region begins to interact with the preexisting negative-polarity flux, and the two regions converge at 0.17 km s^{-1}. In stage 2 reconnection between the interacting opposite-polarity regions causes the formation of a current sheet. The appearance of the bright region between opposite

polarities in the EUV and soft X-ray images is observational evidence of the transition between stage 1 and stage 2. In stage 3 the miniature filament begins to form above the neutral line. The formation of this filament inhibits further reconnection between the opposite-polarity regions temporarily, and in stage 4 a stable magnetic configuration is attained, which results in

the slow buildup of magnetic energy due to the continuing converging motion of the two regions. Eventually, in stage 5, reconnection below the miniature filament causes it to detach and erupt, so that in stage 6 the small two-ribbon flare is seen. The possible rotational motion of the erupting material can be explained by the propagation of released twist that had been stored in the closed-loop field lines of the emerging flux region (as discussed by Canfield et al. 1996). Finally, the approach of the two ribbons at 3.33 km s^{-1} is due to the reconnection of successive field lines below the erupting filament. In this case, the two ribbons also cover the footpoints of the emerging flux region, so that as reconnection proceeds the footpoints of the reconnecting emerging flux become closer and closer together (Canfield et al. 1996). The appearance of detailed structure in the lower ribbon may be evidence of the usual separation of flare ribbons at the footpoints of the other field lines, i.e., those that were formed by reconnection between the positive polarity of the emerging flux region and the preexisting negative polarity.

Although a detailed comparison between the observational quantities and the physical parameters of numerical simulations is beyond the scope of the present paper, it is instructive to make some estimates to confirm that our interpretation is indeed quantitatively plausible. To this end, we first estimate the thermal energy content of the small flare via $E_{\text{th}} = 3k_{\text{B}}T_eN_eL^3$, where N_e is the electron density, T_e is the electron temperature, k_{B} is Boltzmann's constant, and L is the length such that L^3 is the volume. Therefore, we assume that the volume depth is the same as the square root of the surface area, and L is taken to be 7″8 (see § 3.1). The electron temperature is taken to be on the order of 5 MK. We also assume that the electron density is in the range 10^9–10^{10} cm^{-3}. These values are those typically found for small flares from *Yohkoh* SXT observations (Shimizu 1995). As a result, we derive a value of 3.8×10^{26}–3.8×10^{27} ergs. Assuming a coronal magnetic field strength of about 100 G, we then derive the magnetic energy content via the relation $E_{\text{mag}} = (B^2/8\pi)L^3$, where B is the coronal magnetic field strength. This approximation leads to $E_{\text{mag}} = 7.2 \times 10^{28}$ ergs, which is ∼19–190 times larger than the thermal energy estimate, i.e., we can conclude that the magnetic energy released through reconnection is sufficient to account for the thermal energy of the small flare. Finally, we

estimate whether sufficient energy could be stored in the short time between the filament formation and subsequent eruption. The rate of increase of magnetic energy in an emerging flux region can be estimated from $E_{\text{ef}} = L^2(B^2/4\pi)v$, where L^2 is the area and v is the rising speed of the emerging flux. As discussed by Shibata et al. (1989), the rising speed of emerging flux at the photospheric level is on the order of ∼1 km s^{-1}. Therefore, assuming the same quantities as before for the other parameters, we estimate a value of 3.2×10^{25} ergs s^{-1}. In order to account for the estimated magnetic energy of the flare, this amount of energy must continue to be stored for about 2000 s, i.e., 30–40 minutes. Since the minifilament formed some time before or around 6:30 UT and was clearly visible by 6:47 UT, and the two-ribbon flare peaked around 7:17 UT, we conclude that sufficient time elapsed for enough magnetic energy to be stored to explain the characteristics of this small flare.

The morphological model of Figure 11 is an application of the plasmoid-induced reconnection model, presented by Shibata (1996, 1998, 1999; see especially Fig. 5 of Shibata 1998), and can explain the observed features and dynamics of the small-scale two-ribbon flare associated with the eruptive miniature filament on 2001 July 14. As such, these observational results and this particular interpretation suggest that a unified magnetic reconnection model may be able to explain all scales of solar flares.

REFERENCES

Canfield, R. C., Readon, K. P., Leka, K. D., Shibata, K., Yokoyama, T., & Shimojo, M. 1996, ApJ, 464, 1016
Cargill, P., & Priest, E. R. 1983, ApJ, 266, 383
Carmichael, H. 1964, in The Physics of Solar Flares ed. W. N. Hess (NASA SP-50; Washington: NASA), 451
Cliver, E. W. 1983, Sol. Phys., 84, 347
Delaboudiniére, J.-P., et al. 1995, Sol. Phys., 162, 291
Falconer, D. A., Moore, R. L., Porter, J. G., & Hathaway, D. H. 2003, ApJ, 593, 549
Forbes, T. G., & Priest, E. R. 1982, Sol. Phys., 81, 303
Hermans, L. M., & Martin, S. F. 1986, in Coronal and Prominence Plasmas, ed. A. I. Poland (NASA CP-2442; Washington: NASA), 369
Hirayama, T. 1974, Sol. Phys., 34, 323
Kopp, R. A., & Pneuman, G. W. 1976, Sol. Phys., 50, 85
Kurokawa, H., Hanaoka, Y., Shibata, K., & Uchida, Y. 1987, Sol. Phys., 108, 251
Kurokawa, H., Ishiura, K., Kimura, G., Nakai, Y., Kitai, R., Funakoshi, Y., & Shinkawa, T. 1995, J. Geomagn. Geoelectr., 47, 1043
Labonte, B. J. 1979, Sol. Phys., 61, 283
Martens, P. C. H., & Kuin, N. P. M. 1989, Sol. Phys., 122, 263

Moore, R. L., Falconer, D. A., Porter, J. G., & Suess, S. T. 1999, ApJ, 526, 505
Moore, R. L., & Roumeliotis, G. 1992, in Eruptive Solar Flares, ed. Z. Svestka, B. V. Jackson, & M. E. Machado (New York: Springer), 69
Moore, R. L., Tang, F., Bohlin, J. D., & Golub, L. 1977, ApJ, 218, 286
Scherrer, P. H., et al. 1995, Sol. Phys., 162, 129
Shibata, K. 1996, Adv. Space Res., 17(4–5), 9
———. 1998, in Proc. Observational Plasma Astrophysics: Five Years of Yohkoh and Beyond, ed. T. Watanabe, T. Kosugi, & A. C. Sterling (Dordrecht: Kluwer), 187
———. 1999, Ap&SS, 264, 129
Shibata, K., Tajima, T., Steinolfson, R. S., & Matsumoto, R. 1989, ApJ, 345, 584
Shimizu, T. 1995, PASJ, 47, 251
Sturrock, P. A. 1966, Nature, 211, 695
Svestka, Z., & Cliver, E. W. 1992, in Eruptive Solar Flares, ed. Z. Svestka, B. V. Jackson, & M. E. Machado (New York: Springer), 1
Tsuneta, S., et al. 1991, Sol. Phys., 136, 37
Wang, J., Li, W., Denker, C., Lee, C., Wang, H., Goode, P. R., McAllister, A., & Martin, S. F. 2000, ApJ, 530, 1071